Journal of Power Sources 224 (2013) 180–194

Contents lists available at SciVerse ScienceDirect

Journal of Power Sources

journal homepage: www.elsevier.com/locate/jpowsour

Extension of physics-based single particle model for higher charge–discharge rates

Saeed Khaleghi Rahimian, Sean Rayman, Ralph E. White*

Department of Chemical Engineering, University of South Carolina, Swearingen Engineering Center, 301 Main Street, Columbia, SC 29208, USA

HIGHLIGHTS

- We extended the physics-based single particle model for higher charge–discharge rates up to 5C.
- The improved single particle (ISP) model was compared with full-order pseudo two dimensional (P2D) model.
- The ISP model could predict the P2D model results up to 5C while the simulation time was reduced by a factor about 5.

ARTICLE INFO

Article history:
Received 9 July 2012
Received in revised form
21 September 2012
Accepted 23 September 2012
Available online 28 September 2012

Keywords:
Li ion battery
Model order reduction
Single particle model
Polynomial approximation

ABSTRACT

An isothermal reduced order physics-based Li ion battery model is developed by incorporating solution phase charge and material balances into single particle (SP) model. Li ion concentration and potential profiles in electrolyte phase are approximated by polynomial functions. A cubic polynomial is used for electrolyte concentration and potential inside electrodes, while separator liquid phase potential and concentration are estimated by parabolas. Diffusion inside solid particles is also simplified using an approximate solution based on analytical solution for the solid concentration. Applying the aforementioned reduction techniques decreases the degree of freedom of full order model by more than 100, while the cell voltage relative error of proposed model is less than 1% at different charge–discharge rates up to 5C.

1. Introduction

Due to high energy density of Li ion cells with respect to other kind of batteries (three to four times of Lead acid and Nickel cadmium and twice of Nickel metal hydride) rechargeable Li ion batteries are used extensively in different markets and applications ranging from consumer electronics (e.g. laptops, cell phones) to automotive (e.g. Hybrid Electrical Vehicles) and aerospace (e.g. satellite power sources) [1]. However, Li ion cells are unforgiving if operated outside of tight safe operating area [2]. In order to guarantee safe charge–discharge operations of a Li ion cell, most battery systems consist of a battery management system (BMS) to control charging–discharging [2]. The core of a BMS is a battery model that finds the relationship between currents and voltages measured at terminals [3].

Li ion cell models are categorized into two main groups. The first type is empirical approaches that rely on capacitor–resistor networks such as equivalent circuit model (ECM) [4]. Due to simplicity and low computational burden, empirical models have been used widely in online implementations [4]. However, physical insight of the cell is neglected, resulting in prediction errors when used over a broad operating region [3]. The second type includes physics-based models like Pseudo Two Dimensional (P2D) [5,6] where distribution of essential states inside the cell (e.g. solid and liquid phase Li ion concentrations and potentials) along cell sandwich is obtained by solving material and charge balances. Thus, physics-based models can be applied in different operation modes and also capacity fade phenomena are included in the model without any difficulty [7]. Nevertheless, the complexity and computational cost restricts the use of these models for onboard applications.

In order to make rigorous physics-based models more computationally efficient, various reduced models have been proposed [8,9,11–16]. The most simplified model developed by Atlung et al. [8] and later extended by Haran et al. [9] is single particle (SP) model where each electrode is represented by a single spherical particle and Li ion concentration and potential inside electrolyte phase are neglected. Although the SP model computation time is comparable with empirical ECM [10], it is limited for low rate operations (e.g. ≤1.0C) [11]. V.R. Subramanian et al. approximated

* Corresponding author. Tel.: +1 803 777 3270; fax: +1 803 777 0973.
E-mail address: white@cec.sc.edu (R.E. White).

0378-7753/$ – see front matter © 2012 Elsevier B.V. All rights reserved.
http://dx.doi.org/10.1016/j.jpowsour.2012.09.084

microscale diffusion equation in a spherical electrode particle based on polynomial profile [12]. They coupled the approximated solution with governing equations for the macroscale to predict the cell voltage as well as electrolyte concentration. Although it was shown that the number of differential algebraic equations (DAEs) reduced by order of 10, the resulting DAE is still large. In the next work by V.R. Subramanian et al., the full order DAE system was reduced further by approximating electrolyte concentrations inside electrodes and separator using polynomial functions [13]. They showed that approximated solutions for different quantities such as electrolyte concentrations and potential agreed well with full order profiles under 1C discharge rate. However, uniform electrolyte current densities were assumed in each electrode. As we will show later in this paper, this assumption is true only for low charge–discharge rates.

A physics-based reduced-order model was proposed by L. Cai and R.E. White based on proper orthogonal decomposition [14]. There were 50 equations in the reduced model (compared to 14,580 equations in high-order dimensional discrete model) that saved the computational time of the rigorous model by a factor about 7. Smith et al. developed a low order electrochemical model under assumptions of quasi-linear behavior (i.e., constant electrolyte properties and linearized Butler Volmer (BV) kinetics) and reaction current decoupled from electrolyte concentration [15]. They reduced a full order impedance transfer matrix to a 12th order state variable model that predicted the cell voltage to within 1% for pulse and constant current profiles at rates up to 50 C. However, the validity of the reduced model was lost when the electrolyte became depleted ($C_e < 0.15\ C_{e,0}$). Smith et al.'s model was further simplified by D. Di Domenico et al. assuming a constant electrolyte concentration and neglecting the solid concentration distribution along each electrode (resulting in constant current density in BV kinetics) [16]. Their reduced model is similar but higher order than SP model. Recently, T.-S. Dao et al. presented a simplified model using a volume average technique for solid phase concentration and Galerkin's approximation for electrolyte phase concentration and potential [17]. The current density was also assumed to be constant along each electrode. They obtained a set of $2N + 10$ (N is number of node points for Galerkin's approximation) DAEs where $N = 4$ resulted a reduced model in good agreement with rigorous model for 1 C discharge rate.

In this paper, the isothermal SP model without capacity fade [10] is improved to predict the cell voltage at higher charge–discharge rates up to 5C where the Li ion concentration in electrolyte phase (near to cathode/anode current collector during discharge/charge) depletes near to zero ($C_e \sim 0.001\ C_{e,0}$). Distribution of electrolyte concentration and potential along electrodes and separator are incorporated with the SP model equations by using polynomial approximations for the electrolyte concentrations and potentials. The new efficient reduced model consists of only 13 DAEs where cubic and quadratic polynomials are applied for solution phase transport and conduction in electrodes and separator respectively. As mentioned in Ref. [13] the proposed method is slightly different from standard collocation procedures because governing equations are also volume averaged to find polynomial coefficients. In order to enhance the accuracy of solid phase surface concentration, the volume average technique used in Ref. [10] is replaced by an approximated solution developed by M. Guo and R.E. White [18]. Comparison of constant current charge–discharge data obtained by full order P2D with improved single particle (ISP) model shows that there is a good agreement between the reduced and the rigorous models while the computation time of the new model is greatly less than the full model (a factor of 5).

2. Physics-based model

In this section, the assumptions and governing equations of full order P2D model for Li ion concentrations and potentials inside solid and solution phases are first presented. Then, the underlying assumptions and restrictions of simplified SP model are addressed. Finally, the SP model is extended to higher rates by coupling the electrolyte charge and material balances to solid phase diffusion. In all models, the BV expression is used to predict the rates of Li ions intercalation/deintercalation reactions.

2.1. Pseudo two dimensional model

Fig. 1 presents a schematic of a Li ion cell composing of two porous electrodes (solid matrix inside an electrolyte solution) and a separator (electrolyte solution). Most physics-based full order Li-ion cell models rely on the rigorous model of Doyle et al. [5] and T.F. Fuller et al. [6]. Transport of Li ions in the electrolyte phase is considered only in x direction (i.e. from the cathode through the separator into the anode during charge and vice versa during discharge) since the lengths of the cell in y and z directions are much greater than the cell thickness (>1000). In the solid phase Li ions are assumed to react at the surface and move only in r direction. Thus, simulation of the cell can be regarded as a packed bed reactor model. In addition to material balances of Li ions inside liquid and solid phases, charge balances for each phase are required in order to obtain the potential distribution across the cell. Hence, there are four quantities describing the cell electrochemical behavior including solid and electrolyte Li ion concentration and potential. These variables are coupled by a charge-transfer kinetic resistance at the particle surface. In the following, governing equations and assumptions are presented.

2.1.1. Solid concentration

Li ions travel inside spherical solid particles by diffusion process given by the Fick's second law:

$$\frac{\partial C_{s,i}}{\partial t} = \frac{D_{s,i}}{r^2}\frac{\partial}{\partial r}\left(r^2\frac{\partial C_{s,i}}{\partial r}\right) \quad i = p, n \tag{1a}$$

with the initial and boundary conditions:

$$\begin{aligned} &C_{s,i}(r, t = 0) = C_{s,i,0} \quad 0 \le r \le R_i \\ &\left.\frac{\partial C_{s,i}}{\partial r}\right|_{r=0} = 0 \qquad t>0 \\ &-D_{s,i}\left.\frac{\partial C_{s,i}}{\partial r}\right|_{r=R_i} = J_i(x, t) \end{aligned} \tag{1b}$$

where J_i is the pore wall flux at the interface between electrolyte and particles. $D_{s,i}$, the diffusion coefficient of Li ions inside solid particles, is a constant.

2.1.2. Solid potential

The potential distribution in the solid phase of each electrode is obtained by Ohm's law together with the boundary conditions at two ends of the cell and the electrode/separator interfaces:

$$\sigma_{\text{eff},i}\frac{\partial^2\phi_i}{\partial x^2} = a_i F J_i(x, t) \quad i = p, n$$

$$\text{Cathode}: \quad -\sigma_{\text{eff,p}}\left.\frac{\partial\phi_p}{\partial x}\right|_{x=0} = I_{\text{app}} \qquad \left.\frac{\partial\phi_p}{\partial x}\right|_{x=L_p} = 0 \tag{2}$$

$$\text{Anode}: \quad \left.\frac{\partial\phi_n}{\partial x}\right|_{x=L_p+L_s} = 0 \qquad \phi_n|_{x=L} = 0$$

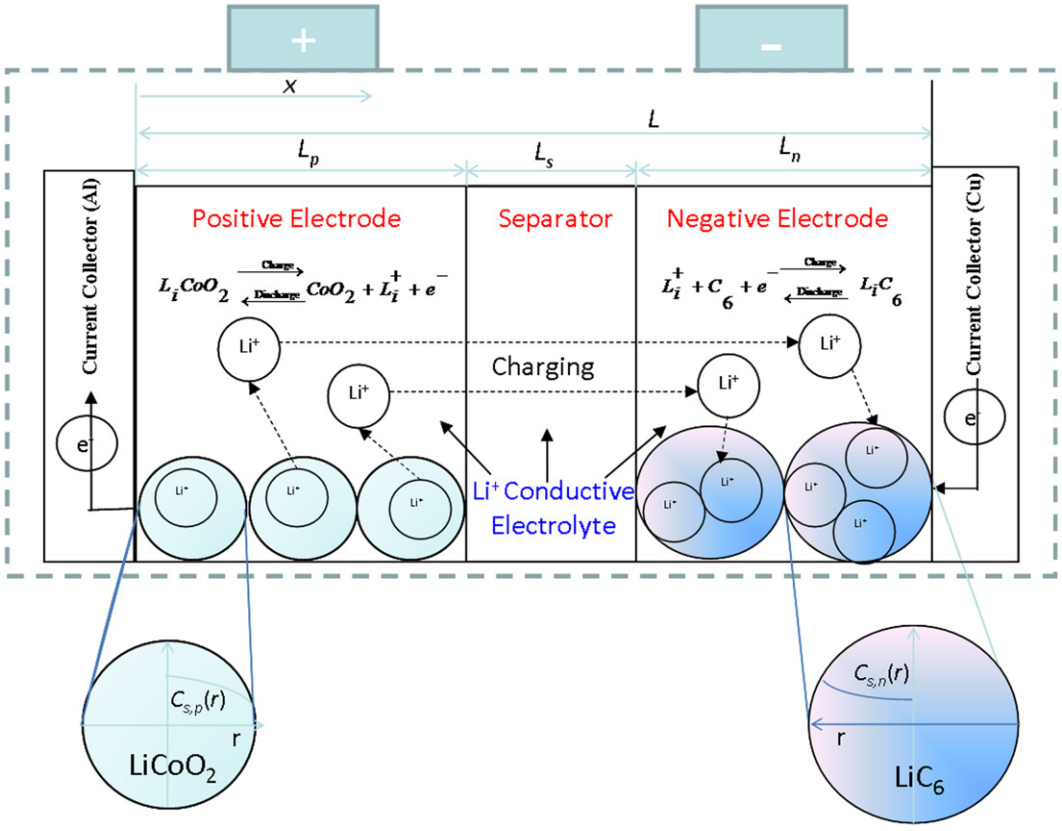

Fig. 1. Schematic of a Li ion cell.

where $\sigma_{\text{eff,i}}$ is constant effective solid conductivity and a_i, specific interfacial area, is determined by:

$$a_i = \frac{3\left(1-\varepsilon_i-\varepsilon_{f,i}\right)}{R_i}$$

where $\varepsilon_{\text{f,i}}$ is volume fraction of fillers. The charge flux at the current collector/cathode interface is equal to the applied current to the cell while there is no charge flux at the electrode/separator interfaces. The potential at the current collector/anode interface is arbitrary set to zero.

2.1.3. Electrolyte concentration

The material balance on the salt in the electrolyte phase for different regions is obtained by assuming concentrated solution theory (a binary salt plus solvent) [19]:

- Cathode:

$$\frac{\partial C_{\text{e,p}}}{\partial t} = \frac{1}{\varepsilon_{\text{p}}}\frac{\partial}{\partial x}\left(D_{\text{e,p}}\frac{\partial C_{\text{e,p}}}{\partial x}\right) + \frac{\left(1-t_+^0\right)a_{\text{p}}J_{\text{p}}(x,t)}{\varepsilon_{\text{p}}} \tag{3a}$$

- Separator:

$$\frac{\partial C_{\text{e,s}}}{\partial t} = \frac{1}{\varepsilon_{\text{s}}}\frac{\partial}{\partial x}\left(D_{\text{e,s}}\frac{\partial C_{\text{e,s}}}{\partial x}\right) \tag{3b}$$

- Anode:

$$\frac{\partial C_{\text{e,n}}}{\partial t} = \frac{1}{\varepsilon_{\text{n}}}\frac{\partial}{\partial x}\left(D_{\text{e,n}}\frac{\partial C_{\text{e,n}}}{\partial x}\right) + \frac{\left(1-t_+^0\right)a_{\text{n}}J_{\text{n}}(x,t)}{\varepsilon_{\text{n}}} \tag{3c}$$

where the transference number of Li ions, t_+^0, is assumed to be constant and the effective diffusion coefficient of the lithium salt, $D_{\text{e,i}}$, depends on the electrolyte concentration, temperature, porosity and Bruggeman number [20]

$$\begin{aligned} D_{\text{e},i} &= \varepsilon_i^{\text{brugg}_i} D_i, \quad i = p,s,n \\ D_i &= 10^{-4.43-\frac{54}{T-229-5.0\times10^3 C_{\text{e},i}(x,t)}-0.22\times10^3 C_{\text{e},i}(x,t)} \end{aligned} \tag{4}$$

The following boundary conditions are applied for the electrolyte concentration:

- No mass flux at two ends of the cell in x-direction

$$-D_{\text{e,p}}\frac{\partial C_{\text{e,p}}(x,t)}{\partial x}\bigg|_{x=0} = 0 \tag{5a}$$

$$-D_{e,n}\frac{\partial C_{e,n}(x,t)}{\partial x}\bigg|_{x=L} = 0 \tag{5b}$$

- Continuity of the concentration and the flux at the cathode/separator interface:

$$C_{e,p}(L_p,t) = C_{e,s}(L_p,t) \tag{5c}$$

$$-D_{e,p}\frac{\partial C_{e,p}(x,t)}{\partial x}\bigg|_{x=L_p} = -D_{e,s}\frac{\partial C_{e,s}(x,t)}{\partial x}\bigg|_{x=L_p} \tag{5d}$$

- Continuity of the concentration and the flux at the separator/anode interface:

$$C_{e,s}(L_p+L_s,t) = C_{e,n}(L_p+L_s,t) \tag{5e}$$

$$-D_{e,s}\frac{\partial C_{e,s}(x,t)}{\partial x}\bigg|_{x=L_p+L_s} = -D_{e,n}\frac{\partial C_{e,n}(x,t)}{\partial x}\bigg|_{x=L_p+L_s} \tag{5f}$$

2.1.4. Electrolyte potential

The variation in electrolyte potential inside the cell is determined by applying Ohm's law having assumed the electrolyte is an ideal solution:

- Cathode:

$$-\frac{\partial}{\partial x}\left(k_{e,p}\frac{\partial \phi_{e,p}}{\partial x}\right) + \beta\frac{\partial}{\partial x}\left(\frac{k_{e,p}}{C_{e,p}}\frac{\partial C_{e,p}}{\partial x}\right) = a_p F J_p(x,t) \tag{6a}$$

- Separator:

$$-\frac{\partial}{\partial x}\left(k_{e,s}\frac{\partial \phi_{e,s}}{\partial x}\right) + \beta\frac{\partial}{\partial x}\left(\frac{k_{e,s}}{C_{e,s}}\frac{\partial C_{e,s}}{\partial x}\right) = 0 \tag{6b}$$

- Anode:

$$-\frac{\partial}{\partial x}\left(k_{e,n}\frac{\partial \phi_{e,n}}{\partial x}\right) + \beta\frac{\partial}{\partial x}\left(\frac{k_{e,n}}{C_{e,n}}\frac{\partial C_{e,n}}{\partial x}\right) = a_n F J_n(x,t)$$

where β is equal to $2R_gT(1-t_+^0)/F$ and the specific conductivity is a function of the electrolyte concentration, temperature, porosity and Bruggman number [20]:

$$\begin{aligned} &k_{e,i} = \varepsilon_i^{brugg_i}K_i, \quad i = p,s,n \\ &K_i = 10^{-4}C_{e,i}\left(\begin{array}{l}-10.5+0.668\times10^{-3}C_{e,i}+0.494\times10^{-6}C_{e,i}^2+0.074T-1.78\times \\ 10^{-5}C_{e,i}T-8.86\times10^{-10}C_{e,i}^2T-6.96\times10^{-5}T^2+2.80\times10^{-8}C_{e,i}T^2\end{array}\right)^2 \end{aligned} \tag{7}$$

The following boundary conditions are used for the electrolyte potential inside the cell:

- No charge flux at two end of the cell:

$$-k_{e,p}\frac{\partial \phi_{e,p}}{\partial x}\bigg|_{x=0} = 0 \tag{8a}$$

$$-k_{e,n}\frac{\partial \phi_{e,n}}{\partial x}\bigg|_{x=L} = 0 \tag{8b}$$

- Continuity of potential and charge flux at the cathode/separator interface:

$$\phi_{e,p}(L_p,t) = \phi_{e,s}(L_p,t) \tag{8c}$$

$$-k_{e,p}\frac{\partial \phi_{e,p}}{\partial x}\bigg|_{x=L_p} = -k_{e,s}\frac{\partial \phi_{e,p}}{\partial x}\bigg|_{x=L_p} \tag{8d}$$

- Continuity of the potential and charge flux at the interface separator/anode:

$$\phi_{e,s}(L_p+L_s,t) = \phi_{e,n}(L_p+L_s,t) \tag{8e}$$

$$-k_{e,s}\frac{\partial \phi_{e,s}}{\partial x}\bigg|_{x=L_p+L_s} = -k_{e,n}\frac{\partial \phi_{e,n}}{\partial x}\bigg|_{x=L_p+L_s} \tag{8f}$$

2.1.5. Pore wall flux

The BV kinetic expression is used to predict the rates of the Li ion deintercalation/intercalation reactions for each electrode:

$$\begin{aligned} J_i(x,t) = 2k_i\Big(&C_{s,max,i} \\ &-x_{s,surf,i}C_{s,max,i}\Big)^{0.5}\Big(x_{s,surf,i}C_{s,max,i}\Big)^{0.5}C_{e,i}^{0.5}\sinh\left(\frac{0.5F}{R_gT}\eta_i\right) \end{aligned} \tag{9}$$

The electrode overpotential for the lithium ion intercalation/deintercalation reactions is given by:

$$\eta_i = \phi_i - \phi_{e,i} - U_i\Big(x_{s,surf,i}\Big) \tag{10}$$

where U_i denotes electrode's open circuit potential [7]. The cell voltage is calculated by the following equation:

$$V_{\text{cell}} = \phi_{\text{p}}\big|_{x=0} - \phi_{\text{n}}|_{x=L} \tag{11}$$

2.1.6. DAE system

In order to solve the system of coupled PDEs of the full order model, discretization along x axis in the electrodes and the separator in association with discretization along r axis for the solid diffusion are required. The P2D model is solved in COMSOL Inc. Multiphysics 3.5a by using 70, 25, 74 elements along x axis for cathode, separator and anode respectively. The particles in solid phase are divided into 200 elements. If the element type is selected as Lagrange-Quadratic (default), the model consists of 2690 degrees of freedom. The model parameters used in this study are listed in Table 1.

2.2. Single particle model

SP model considers each electrode as a single spherical particle whose area represents the porous electrode active surface area. That is, it is assumed that all of the particles in an electrode behave the same way and that the current being passed through the electrode is distributed uniformly over all of the particles. Moreover, the variation of electrolyte concentration and potential with position and time are ignored. Therefore, the system of full order PDEs is reduced to two solid diffusion PDEs (Eq. (1)) in which each electrode regarded as spherical particles. The solid diffusion equation can also be simplified by applying a volume average technique where a polynomial is used to approximate the concentration profile inside the particle [21]. The PDE and boundary conditions in Eq. (1) are converted to the following DAE system using a parabolic polynomial approximation:

Table 1
Pseudo two dimensional model parameters.

Parameter	Value	Unit
$C_{\text{e},0}$	1000	mol m^{-3}
k_{p}	6.667e-11	m$^{2.5}$mol$^{-0.5}$s^{-1}
k_{n}	1.764e-11	m$^{2.5}$ mol$^{-0.5}$ s^{-1}
R_{p}	8.5e-6	m
R_{n}	12.5e-6	m
$D_{\text{s,p}}$	1e-11	m^2 s^{-1}
$D_{\text{s,n}}$	5.5e-14	m^2 s^{-1}
$C_{\text{s,max,p}}$	51,555	mol m^{-3}
$C_{\text{s,max,n}}$	30,555	mol m^{-3}
ε_{p}	0.3	
ε_{s}	0.45	
ε_{n}	0.4382	
$\varepsilon_{\text{f,p}}$	0.15	
$\varepsilon_{\text{f,n}}$	0.0566	
$\sigma_{\text{eff,p}}$	10	S m^{-1}
$\sigma_{\text{eff,n}}$	100	S m^{-1}
L_{p}	70e-6	m
L_{s}	25e-6	m
L_{n}	73.5e-5	m
t_+^0	0.435	
brugg$_{\text{p}}$	1.5	
brugg$_{\text{s}}$	2.3	
brugg$_{\text{n}}$	4.1	
V_{p}	5.894e-6	m^3
V_{n}	6.189e-6	m^3
S_{p}	1.144	m^2
S_{n}	0.75	m^2
T	298.15	K
R_{g}	8.3143	J mol^{-1} K^{-1}
F	96,487	C mol^{-1}
Cell capacity	1.656	Ah
Cathode initial state of charge for charge	0.95	–
Anode initial state of charge for charge	0.05	–
Cathode initial state of charge for discharge	0.465	–
Anode initial state of charge for discharge	0.756	–

$$\begin{cases} \dfrac{\mathrm{d}x_{\text{s,avg},i}}{\mathrm{d}t} = \dfrac{-3J_i^{\text{T}}}{R_i C_{\text{s,max},i}} \\ x_{\text{s,surf},i} = x_{s,avg,i} + \dfrac{-J_i^{\text{T}} R_i}{5D_{\text{s},i} C_{\text{s,max},i}} \end{cases}, i = p, n \tag{12}$$

where J_i^{T} denotes the total flux of Li ions intercalate into or deintercalate from an electrode:

$$\begin{aligned} J_{\text{p}}^{\text{T}} &= \frac{I_{\text{app}}}{FS_{\text{p}}} \\ J_{\text{n}}^{\text{T}} &= \frac{-I_{\text{app}}}{FS_{\text{n}}} \end{aligned} \tag{13}$$

where S_{i} is the electrode total active surface area that can be determined as the product of the specific interfacial area and the electrode volume:

$$S_i = a_i V_i \tag{14}$$

In summary, the solid surface concentration and potential are functions of time only and the electrolyte concentration and potential are constant restricting the model usage for low rate operation ($\leq$1.0C) [11]. The DAEs of SP model can also be solved analytically when the current is constant, the model does not include capacity fade, and cathodic and anodic transfer coefficients are the same ($\alpha = 0.5$) [10].

2.3. Improved single particle model (ISPM)

This section discusses the extension of the SP model to higher charge–discharge rates. Several improvements are made to different quantities including electrolyte concentration and potential, solid phase concentration. Electrodes' potentials and the pore wall flux for higher rates are also addressed.

2.3.1. Electrolyte concentration

One of the error-prone assumptions of SP model is neglecting the variation of solution phase concentration with time and position. Fig. 2 presents the distribution of electrolyte concentration inside the cell obtained by full order model for different discharge rates at the end of discharge where the cell voltage drops below

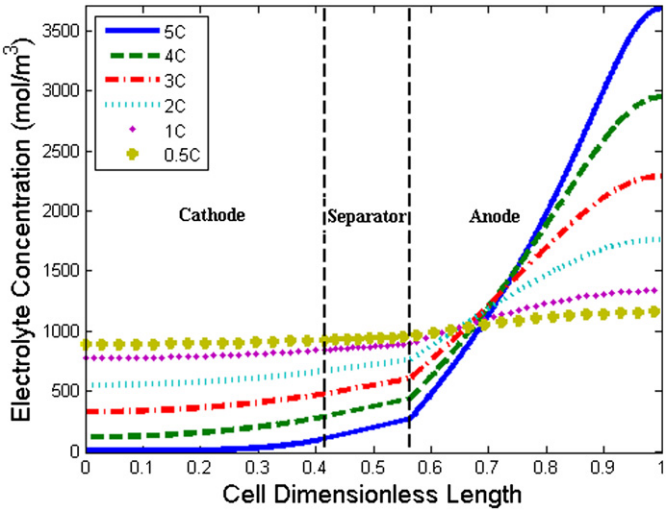

Fig. 2. Electrolyte Li ion concentration inside cell at end of discharge for different rates, P2D model.

3.0 V. The small variation of concentration for lower rates (i.e. 0.5C and 1.0C) validates the SP model constant concentration assumption. However, as the discharge rate increases above 1.0C, the concentration in the electrolyte changes remarkably as shown in Fig. 2. Thus, one has to include the solution phase material balance (Eq. (3)) in SP model. The electrolyte concentration profiles can be approximated by polynomial functions [13]:

$$C_{e,i}(x,t) = a_j(t)x^m + b_j(t)x^{m-1} + \cdots + z_j(t), \quad \begin{cases} i = p,s,n \\ j = 1,2,3 \end{cases} \tag{15}$$

Different polynomial orders can be selected for electrolyte concentrations in the positive electrode, the separator and the negative electrode. In this work, a cubic polynomial is chosen for the electrolyte concentrations inside the electrodes while the separator electrolyte concentration is approximated by a quadratic profile:

$$C_{e,p}(x_p,t) = a_1(t)x_p^3 + b_1(t)x_p^2 + c_1(t)x_p + d_1(t) \tag{16a}$$

$$C_{e,s}(x_s,t) = a_2(t)x_s^2 + b_2(t)x_s + c_2(t) \tag{16b}$$

$$C_{e,n}(x_n,t) = a_3(t)x_n^3 + b_3(t)x_n^2 + c_3(t)x_n + d_3(t) \tag{16c}$$

where x_i is dimensionless length for each region:

$$\begin{cases} x_p = \dfrac{x}{L_p} & \text{for} \quad 0 \le x \le L_p \\ x_s = \dfrac{(x - L_p)}{L_s} & \text{for} \quad L_p \le x \le L_p + L_s \\ x_n = \dfrac{(x - L_p - L_s)}{L_n} & \text{for} \quad L_p + L_s \le x \le L \end{cases} \tag{17}$$

The material balances (Eq. (3)) and boundary conditions (Eq. (5)) can be rewritten using the dimensionless lengths (Eq. (17)):

$$\frac{\partial C_{e,p}}{\partial t} = \frac{1}{L_p^2\varepsilon_p}\frac{\partial}{\partial x_p}\left(D_{e,p}\frac{\partial C_{e,p}}{\partial x_p}\right) + \frac{(1-t_+^0)a_pJ_p(x_p,t)}{\varepsilon_p} \quad (0 \le x_p \le 1) \tag{18a}$$

$$\frac{\partial C_{e,s}}{\partial t} = \frac{1}{L_s^2\varepsilon_s}\frac{\partial}{\partial x_s}\left(D_{e,s}\frac{\partial C_{e,s}}{\partial x_s}\right) \quad (0 \le x_s \le 1) \tag{18b}$$

$$\frac{\partial C_{e,n}}{\partial t} = \frac{1}{L_n^2\varepsilon_n}\frac{\partial}{\partial x_n}\left(D_{e,n}\frac{\partial C_{e,n}}{\partial x_n}\right) + \frac{(1-t_+^0)a_nJ_n(x_n,t)}{\varepsilon_n} \quad (0 \le x_n \le 1) \tag{18c}$$

$$\left.\frac{\partial C_{e,p}(x_p,t)}{\partial x_p}\right|_{x_p=0} = 0 \tag{19a}$$

$$\left.\frac{\partial C_{e,n}(x_n,t)}{\partial x_n}\right|_{x_n=1} = 0 \tag{19b}$$

$$C_{e,p}(x_p = 1,t) = C_{e,s}(x_s = 0,t) \tag{19c}$$

$$C_{e,s}(x_s = 1,t) = C_{e,n}(x_n = 0,t) \tag{19d}$$

$$\frac{\varepsilon_p^{brugg_p}}{L_p}\left.\frac{\partial C_{e,p}(x_p,t)}{\partial x_p}\right|_{x_p=1} = \frac{\varepsilon_s^{brugg_s}}{L_s}\left.\frac{\partial C_{e,s}(x_s,t)}{\partial x_s}\right|_{x_s=0} \tag{19e}$$

$$\frac{\varepsilon_s^{brugg_s}}{L_s}\left.\frac{\partial C_{e,s}(x_s,t)}{\partial x_s}\right|_{x_s=1} = \frac{\varepsilon_n^{brugg_n}}{L_n}\left.\frac{\partial C_{e,n}(x_n,t)}{\partial x_n}\right|_{x_n=0} \tag{19f}$$

The last two equations are a result of the continuity of concentration and temperature at the interfaces and consequently the diffusion coefficient in Eqs. (5d) and (5f).

In order to obtain the electrolyte concentration profile inside the cell, 11 equations are needed to find the 11 polynomial coefficients of Eq. (16). The boundary conditions (Eq. (19)) provide 6 algebraic equations:

$$c_1(t) = 0 \tag{20a}$$

$$3a_3(t) + 2b_3(t) + c_3(t) = 0 \tag{20b}$$

$$a_1(t) + b_1(t) + c_1(t) + d_1(t) - c_2(t) = 0 \tag{20c}$$

$$a_2(t) + b_2(t) + c_2(t) - d_3(t) = 0 \tag{20d}$$

$$\varepsilon L_{ps}(3a_1(t) + 2b_1(t) + c_1(t)) - b_2(t) = 0 \tag{20e}$$

$$\varepsilon L_{sn}(2a_2(t) + b_2(t)) - c_3(t) = 0 \tag{20f}$$

where εL_{ps} and εL_{sn} are given as:

$$\varepsilon L_{ps} = \frac{\varepsilon_p^{brugg_p}L_s}{\varepsilon_s^{brugg_s}L_p}$$

$$\varepsilon L_{sn} = \frac{\varepsilon_s^{brugg_s}L_n}{\varepsilon_n^{brugg_n}L_s}$$

Volume averaging of Eq. (18) yields 3 following ordinary differential equations (ODEs):

$$\begin{aligned} \frac{dC_{e,p,avg}}{dt} &= \frac{1}{L_p^2\varepsilon_p}\left(D_{e,p}\left.\frac{\partial C_{e,p}}{\partial x_p}\right|_{x_p=1}\right) + \frac{(1-t_+^0)a_pI_{app}}{\varepsilon_pFS_p} \\ \frac{dC_{e,s,avg}}{dt} &= \frac{1}{L_s^2\varepsilon_s}\left(D_{e,s}\left.\frac{\partial C_{e,p}}{\partial x_s}\right|_{x_s=1} - D_{e,s}\left.\frac{\partial C_{e,p}}{\partial x_s}\right|_{x_s=0}\right) \\ \frac{dC_{e,n,avg}}{dt} &= \frac{1}{L_n^2\varepsilon_n}\left(-D_{e,n}\left.\frac{\partial C_{e,n}}{\partial x_n}\right|_{x_n=0}\right) - \frac{(1-t_+^0)a_nI_{app}}{\varepsilon_nFS_n} \end{aligned} \tag{21}$$

where the average concentrations are functions of the polynomial coefficients:

$$\begin{aligned} C_{e,p,avg} &= \frac{1}{4}a_1(t) + \frac{1}{3}b_1(t) + \frac{1}{2}c_1(t) + d_1(t) \\ C_{e,s,avg} &= \frac{1}{3}a_2(t) + \frac{1}{2}b_2(t) + c_2(t) \\ C_{e,n,avg} &= \frac{1}{4}a_3(t) + \frac{1}{3}b_3(t) + \frac{1}{2}c_3(t) + d_3(t) \end{aligned} \tag{22}$$

The two remaining equations can be found by evaluation of the material balances inside the cathode (Eq. (18a)) and the anode (Eq. (18c)) at an interior point along the x direction:

$$\left.\frac{dC_{e,p}}{dt}\right|_{x_p=x_p^1} = \frac{1}{L_p^2\varepsilon_p}\frac{\partial}{\partial x_p}\left(D_{e,p}\frac{\partial C_{e,p}}{\partial x_p}\right)\Bigg|_{x_p=x_p^1} + \frac{(1-t_+^0)a_p J_p^1(t)}{\varepsilon_p} \quad (23a)$$

$$\left.\frac{dC_{e,n}}{dt}\right|_{x_n=x_n^1} = \frac{1}{L_n^2\varepsilon_n}\frac{\partial}{\partial x_n}\left(D_{e,n}\frac{\partial C_{e,n}}{\partial x_n}\right)\Bigg|_{x_n=x_n^1} + \frac{(1-t_+^0)a_n J_n^1(t)}{\varepsilon_n} \quad (23b)$$

where $J_i^1(t)$ $(i=p,n)$ represents the pore wall flux at interior point x_i^1. The optimal location of the interior point within the electrodes is discussed in the Results and discussion section of this manuscript.

2.3.2. Electrolyte potential

The electrolyte potential distribution inside the cell for different discharge rates at the end of discharge is depicted in Fig. 3 illustrating the reason for SP model deviation from P2D model at higher rates (≥1.0C). Thus, consideration of the charge balance in the solution phase is essential, in order to predict the cell voltage at higher rates. The solution phase potential inside each electrode is also approximated by polynomials as follows:

$$\phi_{e,p}(x_p,t) = A_1(t)x_p^3 + B_1(t)x_p^2 + C_1(t)x_p + D_1(t) \quad (24a)$$

$$\phi_{e,n}(x_n,t) = A_3(t)x_n^3 + B_3(t)x_n^2 + C_3(t)x_n + D_3(t) \quad (24b)$$

while the analytical solution of the electrolyte potential in separator is obtained by assuming electrolyte constant specific conductivity. The polynomial coefficients of the electrolyte potential in the anode (i.e., A_3, B_3, C_3, D_3) are determined using two boundary conditions at anode current collector (Eq. (25a,b)), the charge balance at x_n^1 (Eq. (25c)) and volume averaging of both side of the charge balance (Eq. (25d)):

$$\left.\frac{\partial\phi_{e,n}}{\partial x_n}\right|_{x_n=1} = 0 \quad (25a)$$

$$\phi_{e,n}(x_n = 1,t) = 0 \quad (25b)$$

$$-\left.\frac{\partial^2\phi_{e,n}}{\partial x_n^2}\right|_{x_n=x_n^1} + \beta\frac{\partial}{\partial x_n}\left(\frac{1}{C_{e,n}}\frac{\partial C_{e,n}}{\partial x_n}\right)\Bigg|_{x_n=x_n^1} = \frac{a_n F L_n^2 J_n^1(t)}{k_{e,n}} \quad (25c)$$

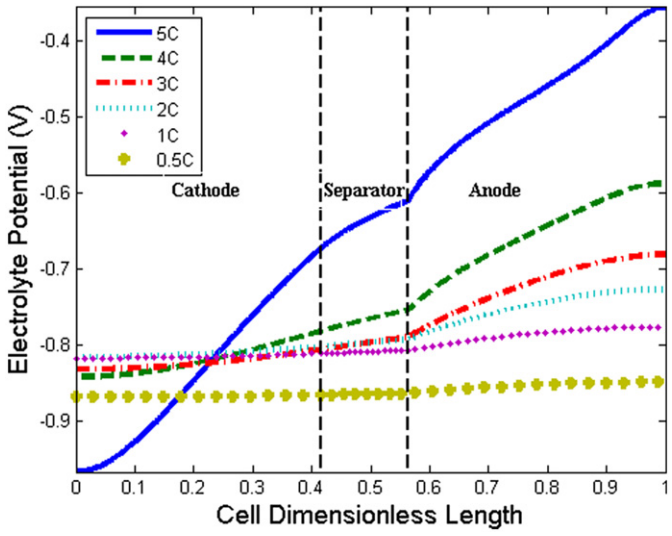

Fig. 3. Electrolyte potential distribution inside cell at end of discharge for different rates, P2D model.

$$k_{e,n}\left.\frac{\partial\phi_{e,n}}{\partial x_n}\right|_{x_n=0} - \frac{\beta k_{e,n}}{C_{e,n}}\left.\frac{\partial C_{e,n}}{\partial x_n}\right|_{x_n=0} = \frac{-I_{app}L_n^2}{V_n} \quad (25d)$$

It is also important to note that in ISP model, the electrolyte potential at the right end of the cell is set to zero (Eq. (25b)) while the potential reference point in P2D model is the solid potential at the right end of the cell. Since the potential difference is considered in the BV kinetic expression, changing the reference point does not affect the results. The charge balance in separator (Eq. (6b)) together with the boundary conditions at the anode/separator interface (Eqs. (8e,f)) can be rewritten as:

$$-\frac{\partial^2\phi_{e,s}}{\partial x_s^2} + \beta\frac{\partial}{\partial x_s}\left(\frac{1}{C_{e,s}}\frac{\partial C_{e,s}}{\partial x_s}\right) = 0 \quad (26a)$$

$$\phi_{e,s}(x_s = 1,t) = \phi_{e,n}(x_n = 0,t) \quad (26b)$$

$$\left.\frac{\partial\phi_{e,s}}{\partial x_s}\right|_{x_s=1} = \frac{1}{\varepsilon L_{sn}}\left.\frac{\partial\phi_{e,n}}{\partial x_n}\right|_{x_n=0} \quad (26c)$$

Substituting the separator concentration polynomial (Eq. (16b)) in the boundary value problem (Eq. (26)), ϕ_{es} is expressed as:

$$\phi_{e,s} = bc_1 - bc_2 - \beta\ln(a_2+b_2+c_2) + x_s\left(bc_2 - \frac{\beta(2a_2+b_2)}{a_2+b_2+c_2}\right) + \beta\ln\left(a_2x_s^2 + b_2x_s + c_2\right) + \frac{\beta(2a_2+b_2)}{a_2+b_2+c_2}$$

where bc_1 and bc_2 are the boundary conditions (Eq. (26b,c)):

$$\begin{cases} bc_1 = D_3 \\ bc_2 = \dfrac{C_3}{\varepsilon L_{sn}} \end{cases}$$

In order to find the cathode electrolyte potential coefficients (i.e., A_1, B_1, C_1 and D_1) boundary conditions at cathode/separator interface (Eq. (27a,b)), boundary condition at the cathode current collector (Eq. (27c)) and the charge balance at x_p^1 (Eq. (27d)) are used:

$$\phi_{e,p}(x_p = 1,t) = \phi_{e,s}(x_s = 0,t) \quad (27a)$$

$$\left.\frac{\partial\phi_{e,p}}{\partial x_p}\right|_{x_s=1} = \frac{1}{\varepsilon L_{ps}}\left.\frac{\partial\phi_{e,s}}{\partial x_s}\right|_{x_s=0} \quad (27b)$$

$$\left.\frac{\partial\phi_{e,p}}{\partial x_p}\right|_{x_p=0} = 0 \quad (27c)$$

$$-\left.\frac{\partial^2\phi_{e,p}}{\partial x_p^2}\right|_{x_p=x_p^1} + \beta\frac{\partial}{\partial x_p}\left(\frac{1}{C_{e,p}}\frac{\partial C_{e,p}}{\partial x}\right)\Bigg|_{x_p=x_p^1} = \frac{a_p L_p^2 F J_p^1(t)}{k_{e,p}} \quad (27d)$$

In deriving Eq. (25c) and Eq. (27d) the solution phase specific conductivity was assumed to be constant in x-domain.

2.3.3. Solid potential

SP model assumes that the electrode potential, ϕ_i, depends on time only. This assumption is still true for higher rates (e.g. 5C) as shown in Fig. 4 for the cathode and anode. High conductivity of the solid versus the electrolyte makes the solid potential variation inside the cell is negligible with respect to the potential change in the solution phase.

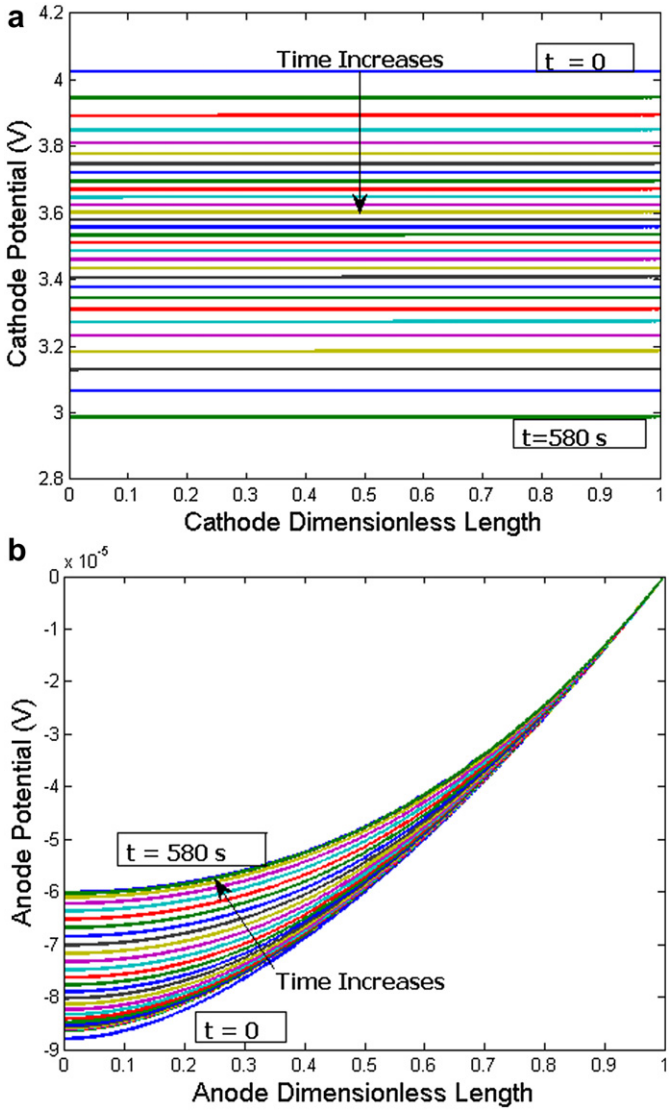

Fig. 4. Potential distribution inside electrodes at 5C discharge, P2D model (a) cathode (b) anode.

2.3.4. Solid concentration

Instead of using volume average technique for approximation of the Li ion concentration inside particles, an approximate solution developed by M. Guo and R.E. White [18] is applied in ISP model. The analytical solution for the solid concentration has the following form:

$$x_s(\bar{r},x,\tau) = x_{s,avg}(x,\tau) + \frac{3}{10}\delta(x,\tau) - \frac{\delta(x,\tau)}{2}\bar{r}^2 + \sum_{n=1}^{\infty}\frac{\sin(\lambda_n\bar{r})}{\bar{r}\sin(\lambda_n)}\left[Q_n(x,\tau) + \frac{2\delta(x,\tau)}{\lambda_n^2}\right]$$

where $x_{s,avg}(x,\tau)$ and $Q_n(x,\tau)$ are calculated by integrating the following ODEs:

$$\frac{dx_{s,avg}(x,\tau)}{d\tau} = -3\delta(x,\tau), \quad x_{s,avg}(x,\tau=0) = x^0_{s,avg} \tag{28a}$$

$$\begin{cases}\dfrac{dQ_n(x,\tau)}{d\tau} = -\lambda_n^2 Q_n(x,\tau) - 2\delta(x,\tau),\ Q_n(x,\tau=0)=0 \\ \lambda_n - \tan(\lambda_n) = 0\end{cases} \text{ for } n=1 \text{ to } \infty \tag{28b}$$

where the dimensionless variables are:

$$\begin{cases}\delta(x,\tau) = \dfrac{J_i(x,t)R_i}{C_{s,max,i}D_{s,i}} \\ \tau = \dfrac{D_{s,i}t}{R_i^2} \\ \bar{r} = \dfrac{r}{R_i}\end{cases}$$

It was shown in Ref. [18] that only a few terms are needed in the analytical solution together with an additional term compensating for the truncation error:

$$\begin{cases}x_{s,surf}(x,\tau) = x_{s,avg}(x,\tau) + \sum_{n=1}^{N} Q_n(x,\tau) + e_N(x,\tau) \\ e_N(x,\tau) = -2\delta(x,\tau)\left(\left(\dfrac{1}{10} - \sum_{n=1}^{N}\dfrac{1}{\lambda_n^2}\right)\left(1-\exp\left(-\lambda_{N+1}^2\tau\right)\right) + \sqrt{\dfrac{\tau}{\pi}}\operatorname{erfc}\left(\lambda_{N+1}\sqrt{\tau}\right)\right)\end{cases} \tag{29}$$

Surface concentration can be expressed explicitly as a function of initial average concentration for constant current charge and discharge where the dimensionless flux is constant ($\delta(x,\tau) = \delta$). In this work, only one term of approximate solution is applied to calculate the surface concentration:

$$x_{s,surf,i}(\tau) = x^0_{s,avg,i} - 3\delta\tau - 2\delta\left(\left(\frac{1}{10} - \frac{1}{\lambda_1^2}\right)\left(1-\exp\left(-\lambda_2^2\tau\right)\right) + \sqrt{\frac{\tau}{\pi}}\operatorname{erfc}\left(\lambda_2\sqrt{\tau}\right)\right) - \frac{2\delta}{\lambda_1^2}\left(1-\exp\left(-\lambda_2^2\tau\right)\right), \quad i = p,n \tag{30}$$

While the total pore wall flux for each electrode (J_i^T) is constant during the constant current charge–discharge, the pore wall flux at electrodes' interior points (J_i^T) vary with time. Thus, Eq. (29) is used to obtain the surface concentration by substituting $x_{s,avg}$ and Q_n calculated by integrating Eq. (28) over time. As a result, if only one term of approximate solution is considered, two ODEs (one for average concentration and one for Q_1) for each surface concentration are needed.

2.3.5. Pore wall flux

In the SP model, the applied current to each particle (electrode) is equal to the total current density over the total electrode active surface area for that electrode. Thus, the variation of the pore wall flux along x axis for each electrode is neglected causing the SP model cell voltage prediction to deviate considerably from the rigorous model at higher rates. Figs. 5 and 6 present the variation of the pore wall flux and current flow in the solution phase, respectively, obtained by the full order model inside the electrodes at a 5C discharge. In most reduced models [13,16,17] the uniform pore wall flux is considered for each electrode resulting in linear variation of the current flow inside the electrode between zero to the applied current. Fig. 6 shows the deviation of the current flow from a straight line especially at the end of discharge. In order to increase the accuracy of the model prediction, one has to apply higher order polynomials for approximation of electrolyte profiles. The BV kinetic can be used at some optimal interior points e.g. (x_n^1, x_p^1) to find the polynomials' coefficients:

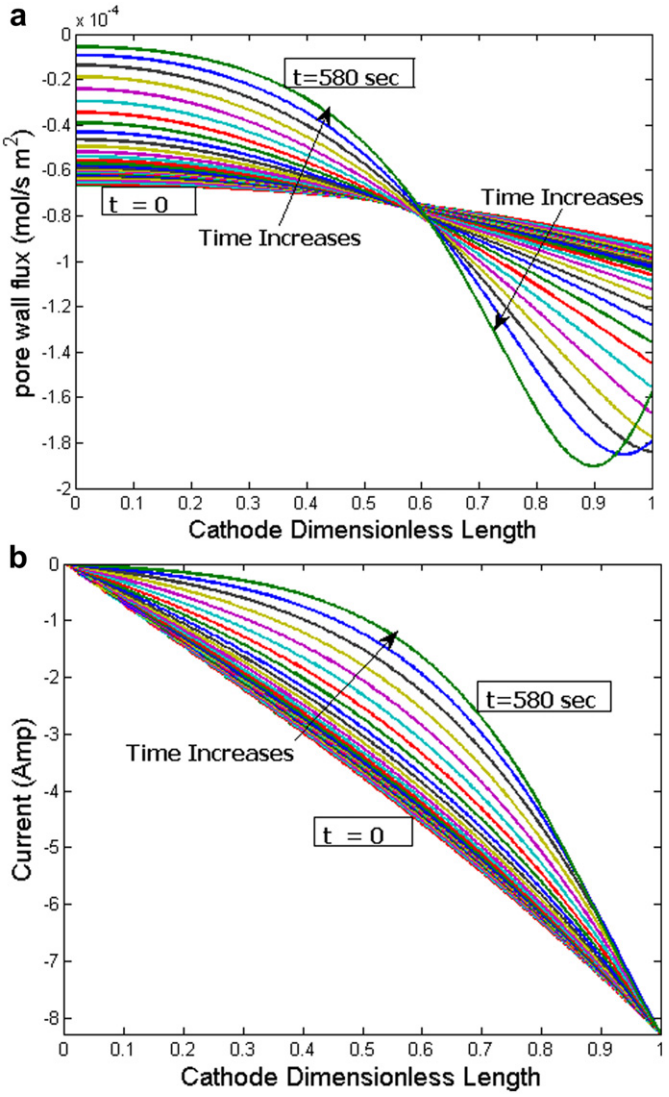

Fig. 5. Cathode pore wall flux (a) and current flow (b) at 5C discharge, P2D model.

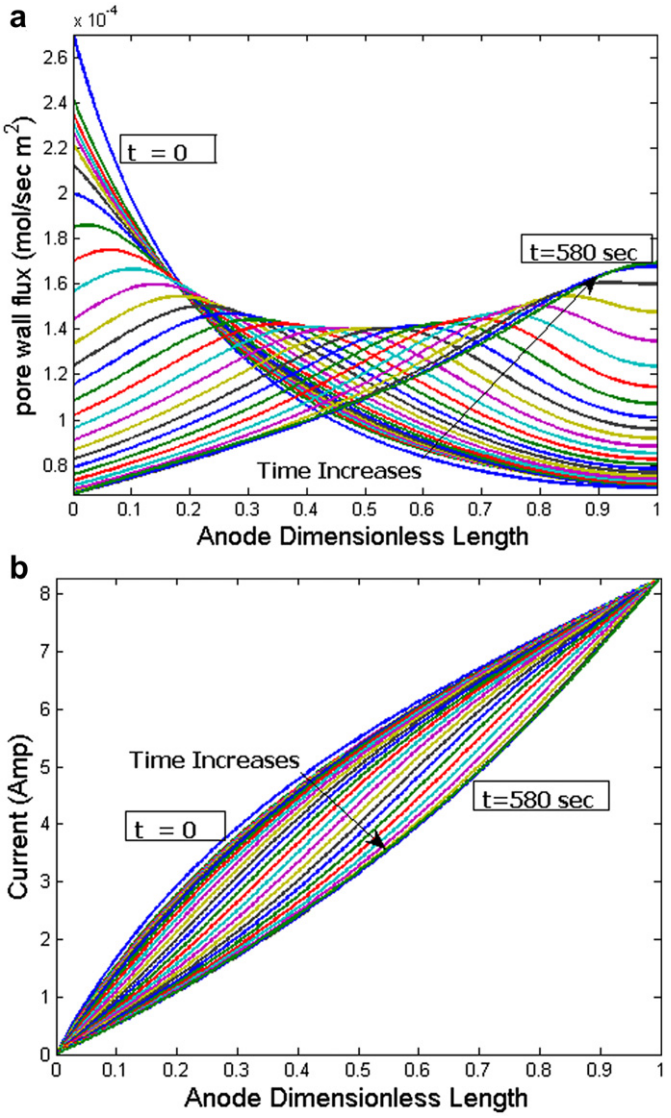

Fig. 6. Anode pore wall flux (a) and current flow (b) at 5C discharge, P2D model.

$$J_i^1(t) = 2k_i\left(C_{s,\max,i} - x^1_{s,surf,i}C_{s,\max,i}\right)^{0.5}\left(x^1_{s,surf,i}C_{s,\max,i}\right)^{0.5}C_{e,i}^{1^{0.5}} \sin h\left(\frac{0.5F}{R_gT}\left(\phi_i - \phi^1_{e,i} - U_i\left(x^1_{s,surf,i}\right)\right)\right) \quad i = p,n \tag{31}$$

where $x^1_{s,surf,i}, C^1_{e,i}$ and $\phi^1_{e,i}$ denote solid surface concentration, solution concentration and electrolyte potential at interior point x_i^1. In order to find the electrodes' potentials, similar to the SP model, the BV expression is also considered for the total pore wall flux for each electrode:

$$J_i^T = 2k_i\left(C_{s,\max,i} - x_{s,surf,i}C_{s,\max,i}\right)^{0.5}\left(x_{s,surf,i}C_{s,\max,i}\right)^{0.5}C^{0.5}_{e,i,avg} \sin h\left(\frac{0.5F}{R_gT}\left(\phi_i - \phi_{e,i,avg} - U_i\left(x_{s,surf,i}\right)\right)\right) \quad i = p,n \tag{32}$$

where $x_{s,surf,i}$ is calculated using Eq. (30) and $C_{e,i,avg}$ and $\phi_{e,i,avg}$ are the volume average electrolyte concentration and potential inside each electrode respectively.

2.3.6. DAE system

Substituting the electrolyte average concentrations (Eq. (22)), polynomial approximation (Eq. (16)), effective diffusion (Eq. (4)) and Eq. (20a) in material balances (Eq. (21)) gives the following ODEs in terms of polynomial coefficients:

$$\begin{aligned}
&\frac{1}{4}\frac{da_1(t)}{dt} + \frac{1}{3}\frac{db_1(t)}{dt} + \frac{dd_1(t)}{dt} = \frac{\varepsilon_p^{brugg_p-1}}{L_p^2}D_p|_{x_p=1}(3a_1(t) + 2b_1(t)) + \frac{(1-t_+^0)a_pI_{app}}{\varepsilon_pFS_p}\\
&\frac{1}{3}\frac{da_2(t)}{dt} + \frac{1}{2}\frac{db_2(t)}{dt} + \frac{dc_2(t)}{dt} = \frac{\varepsilon_s^{brugg_s-1}}{L_s^2}\left(D_s|_{x_s=1}(2a_2(t) + b_2(t)) - D_s|_{x_s=0}b_2(t)\right)\\
&\frac{1}{4}\frac{da_3(t)}{dt} + \frac{1}{3}\frac{db_3(t)}{dt} + \frac{1}{2}\frac{dc_3(t)}{dt} + \frac{dd_3(t)}{dt} = -\frac{\varepsilon_n^{brugg_n-1}}{L_n^2}D_n|_{x_n=0}c_3(t) - \frac{(1-t_+^0)a_nI_{app}}{\varepsilon_nFS_n}
\end{aligned} \tag{33}$$

Eq. (23) is rewritten using the polynomial approximation (Eq. (16)), effective diffusion (Eq. (4)):

$$x_p^{1^3}\frac{da_1(t)}{dt}+x_p^{1^2}\frac{db_1(t)}{dt}+\frac{dd_1(t)}{dt}=\frac{\varepsilon_p^{brugg_p-1}}{L_p^2}g_p\left(x_p^1,t\right)+\frac{(1-t_+^0)a_pJ_p^1(t)}{\varepsilon_pFS_p}$$

$$x_n^{1^3}\frac{da_3(t)}{dt}+x_n^{1^2}\frac{db_3(t)}{dt}+x_n^1\frac{dc_3(t)}{dt}+\frac{dd_3(t)}{dt}=\frac{\varepsilon_n^{brugg_n-1}}{L_n^2}g_n\left(x_n^1,t\right)+\frac{(1-t_+^0)a_nJ_n^1(t)}{\varepsilon_nFS_n} \quad (34)$$

where

$$g_p(x_p,t)=\frac{\partial D_p(x_p,t)}{\partial x_p}\left(3a_1(t)x_p^2+2b_1(t)x_p\right)+D_p(x_p,t)\left(6a_1(t)x_p+2b_1(t)\right)$$

$$g_n(x_n,t)=\frac{\partial D_n(x_n,t)}{\partial x_n}\left(3a_3(t)x_n^2+2b_3(t)x_n+c_3(t)\right)+D_n(x_n,t)(6a_3(t)x_n+2b_3(t))$$

The derivative of $D_e(x_i,t)$ with respect to x_i is determined using the chain rule:

$$\frac{\partial D_i(x_i,t)}{\partial x_i}=\left(\frac{\partial C_{ei}(x_i,t)}{\partial x_i}\right)\left(\frac{-2.7\times10^5}{\left(T-229-5.0\times10^3C_{ei}(x_i,t)\right)^2}-0.22\times10^3\right)(\ln10)D_i(x_i,t)$$

Taking the time derivative of Eq. (20) results in:

$$\begin{cases}\dfrac{dc_1(t)}{dt}=0\\ 3\dfrac{da_3(t)}{dt}+2\dfrac{db_3(t)}{dt}+\dfrac{dc_3(t)}{dt}=0\\ \dfrac{da_1(t)}{dt}+\dfrac{db_1(t)}{dt}+\dfrac{dc_1(t)}{dt}+\dfrac{dd_1(t)}{dt}-\dfrac{dc_2(t)}{dt}=0\\ \dfrac{da_2(t)}{dt}+\dfrac{db_2(t)}{dt}+\dfrac{dc_2(t)}{dt}-\dfrac{dd_3(t)}{dt}=0\\ \varepsilon L_{ps}\left(3\dfrac{da_1(t)}{dt}+2\dfrac{db_1(t)}{dt}+\dfrac{dc_1(t)}{dt}\right)-\dfrac{db_2(t)}{dt}=0\\ \varepsilon L_{sn}\left(2\dfrac{da_2(t)}{dt}+\dfrac{db_2(t)}{dt}\right)-\dfrac{dc_3(t)}{dt}=0\end{cases} \quad (35)$$

Eqs. (33)–(35) are used to find the right hand side of the polynomial coefficients' time derivatives. At least 5 ODEs are required to integrate during charge–discharge time for 5 polynomial coefficients (e.g. $a_1(t)$, $b_1(t)$, $d_1(t)$, $a_2(t)$, $a_3(t)$). The remaining 6 coefficients are evaluated in terms of the 5 coefficients using Eq. (20) as follows:

$$\begin{cases}c_1(t)=0\\ b_2(t)=\varepsilon L_{ps}(3a_1(t)+2b_1(t)+c_1(t))\\ c_2(t)=a_1(t)+b_1(t)+c_1(t)+d_1(t)\\ c_3(t)=\varepsilon L_{sn}(2a_2(t)+b_2(t))\\ d_3(t)=a_2(t)+b_2(t)+c_2(t)\\ b_3(t)=\dfrac{-(3a_3(t)+c_3(t))}{2}\end{cases}$$

Thus, the system of DAEs includes 5 ODEs for 5 electrolyte polynomial coefficients, 4 ODEs (Eq. (28)) for solid average concentration and Q_{1i}, 2 algebraic expressions (Eq. (32)) for pore wall fluxes at the interior points (J_p^1,J_n^1) and 2 algebraic equations (Eq. (31)) for solid phase potentials. Thus, the new reduced-order model consists of 13 DAEs which are solved in COMSOL Inc. Multiphysics 3.5a using Global Equations option to compare the computation time with P2D model. In order to enhance the accuracy of ISP model, higher polynomial order for the solution phase concentrations can be used where the evaluation of the material balances at additional interior points are required to find the polynomial coefficients. Since the BV kinetic expression is evaluated at additional points (Eq. (31)), we are also able to increase the

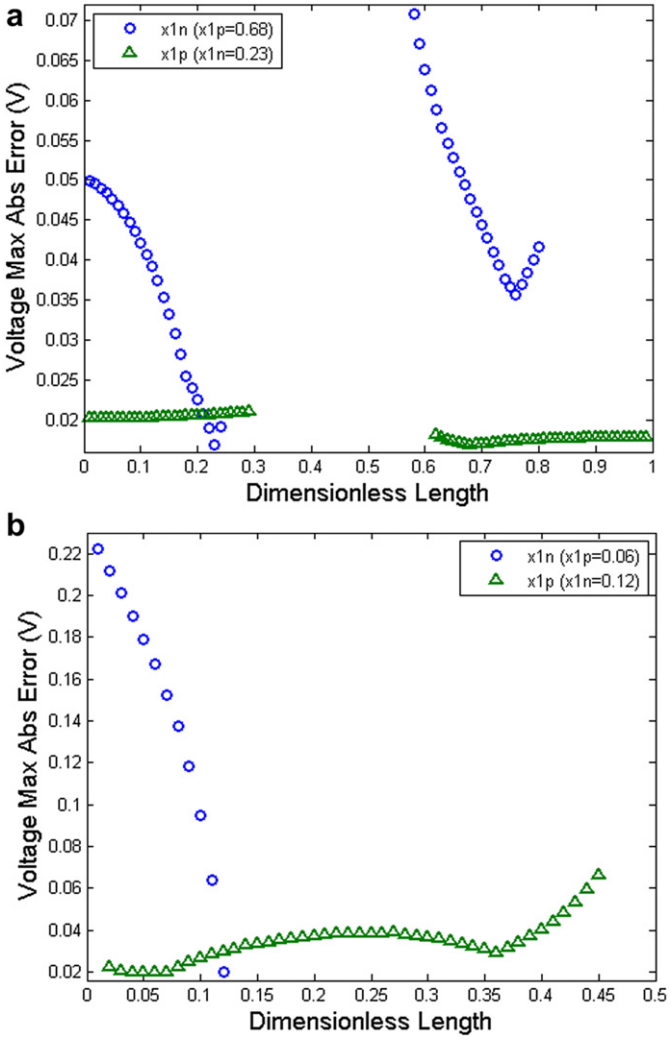

Fig. 7. Cell voltage maximum absolute error versus different interior points inside electrodes, (a) charge (b) discharge.

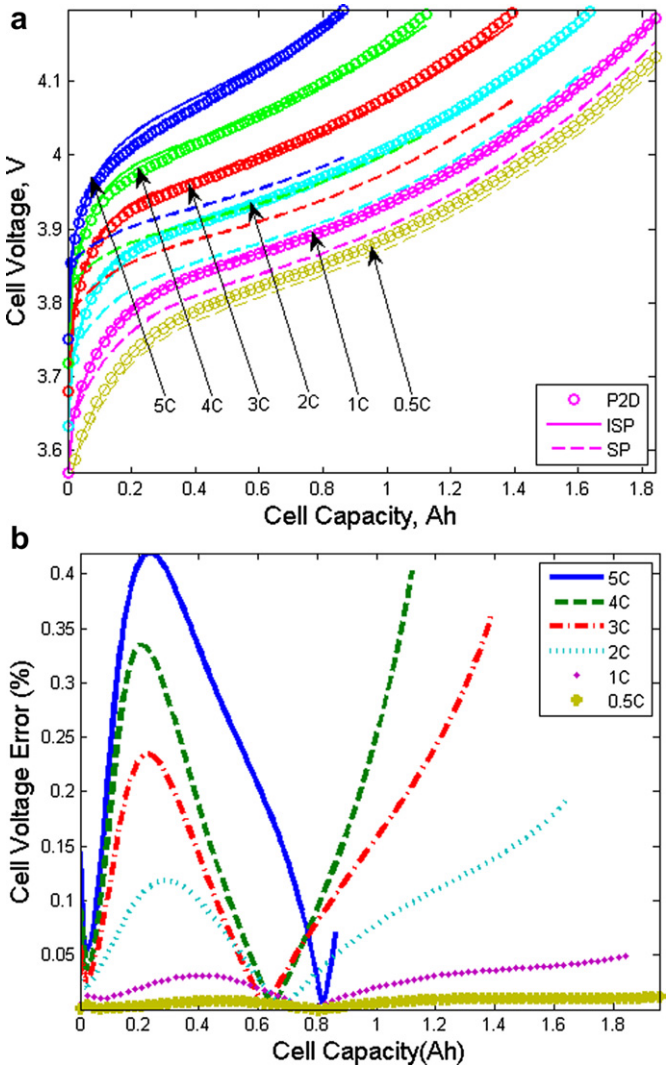

Fig. 8. Cell voltage at different charge rates, (a) comparison of SP and ISP models with P2D model (b) ISP model relative error with respect to P2D model.

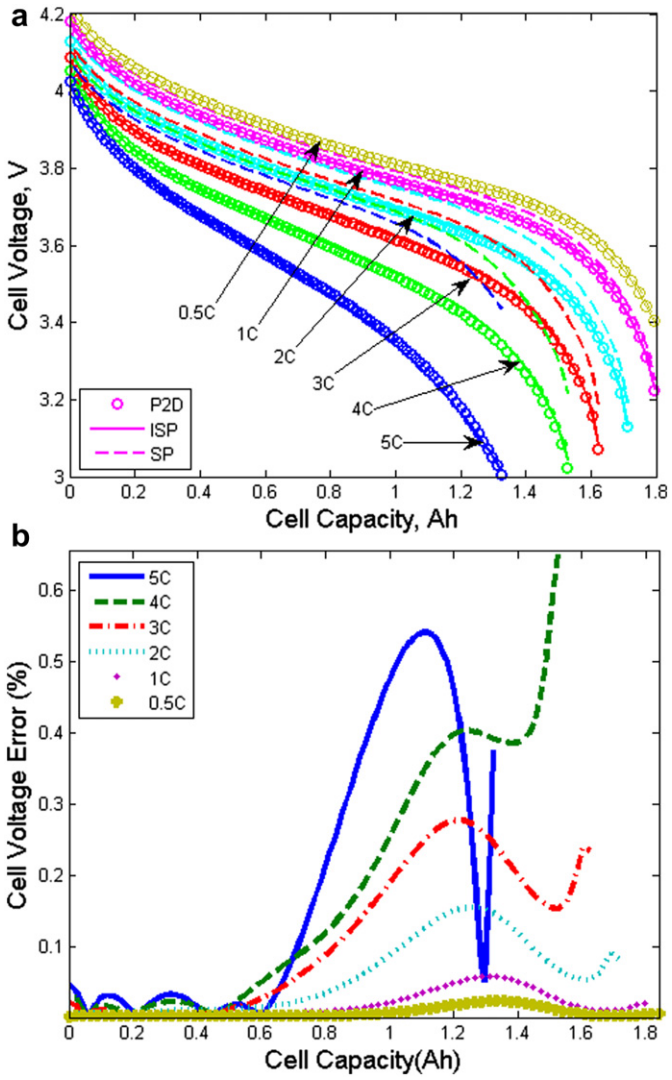

Fig. 9. Cell voltage at different discharge rates, (a) comparison of SP and ISP models with P2D model (b) ISP model relative error with respect to P2D model.

polynomial order of the electrolyte potential as well as Li ion concentrations in solution phase.

3. Results and discussion

This section compares the results of original SP and ISP models with P2D model for different charge–discharge rates. DAEs systems of the models are solved by COMSOL Inc. Multiphysics 3.5a on Windows operating system and the PC is a Dell Precision T7500, with 2 Quad Core 2.53 GHz Zenon Processors CPUs and 12.285 GB of RAM. Note that only one CPU core is involved in numerical simulations (COMSOL processor affinity is set to one CPU (e.g. CPU 0) in Windows Task Manager). Optimal interior points introduced in Eq. (23) are found by applying MATLAB® Global Optimization Toolbox by minimizing the maximum absolute error between ISP and P2D models. The optimal points during charge for all rates (i.e., 1C–5C) are obtained as $x_p^1 = 0.68$ and $x_n^1 = 0.23$ while for all rates (i.e., 1C–5C) during discharge the best interior points are $x_p^1 = 0.06$ and $x_n^1 = 0.12$. The difference in location of the optimal points during charge and discharge is due to the difference in the electrolyte concentration and potential profiles between charge and discharge throughout the cell. In order to show the model sensitivity with different interior points, the cell voltage error for all rates (i.e., 1C–5C) is plotted in Fig. 7 versus different interior points during charge and discharge. The model output does not change considerably when x_p^1 is between 0.01 and 0.29 or 0.62–0.99 during charge (Fig. 7a) (0.017 V ≤ voltage maximum absolute error ≤ 0.021 V) and between 0.02 and 0.39 during discharge (Fig. 7b) (0.02 V ≤ voltage

Table 2
Model results for different charge rates, (a) SP and ISP models voltage errors with respect to P2D model, (b) comparison of ISP and P2D model computation time.

(a)

Model	Voltage sum of squared errors	Voltage maximum absolute error (V)
SP	3.428	0.1995
ISP	0.019	0.0169

(b)

Model	CPU time (s)						
	0.5C	1C	2C	3C	4C	5C	Mean
ISP	2.7	2.3	2.3	1.92	2.1	2.1	2.2
P2D	11.1	10.8	10.1	12.6	13.4	9.2	11.2

Table 3
Model results for different discharge rates, (a) SP and ISP models voltage errors with respect to P2D model, (b) comparison of ISP and P2D model computation time.

(a)

Model	Voltage sum of squared errors	Voltage maximum absolute error (V)
SP	8.912	0.4316
ISP	0.016	0.0198

(b)

Model	CPU time (s)						
	0.5C	1C	2C	3C	4C	5C	Mean
ISP	2.1	2.1	1.9	1.8	2.0	2.5	2.1
P2D	10.0	9.85	10.9	12.5	15.6	14.3	12.2

maximum absolute error ≤ 0.037 V) when x_n^1 is equal to its optimal value. However, the sensitivity of the ISP model with respect to x_n^1 is remarkable specifically during discharge as shown in Fig. 7b (the error is less than 0.05 V only at optimal points, $x_n^1 = 0.12$). Thus, the interior points could be regarded as additional parameters in the new model where one can apply narrow bounds (e.g. [0.01 0.3]) for parameter estimation. The thickness (length) of the cathode, separator, and anode has been made dimensionless in the model and thus the position of the optimal internal points is reported as a dimensionless parameter. However for a different cell capacity, chemistry, or charge/discharge profile the location of the internal points should be optimized. Note that in some regions of Fig. 7 the errors are not shown where either the model DAEs do not converge or the error is outside the plot range.

3.1. Cell voltage

Figs. 8 and 9 compare the cell voltage predicted by ISP model with P2D and SP models for different charge and discharge rates respectively. At lower rates ($\leq$1.0C) SP model prediction agrees well with the rigorous model while the voltage of SP model deviates significantly from the rigorous model voltage as the charge–discharge rates increase above 1C. On the contrary, the ISP model is in good agreement with the full order model at all rates. Tables 2 and 3 summarize the results of the ISP model compared with the SP and P2D models for charge and discharge, respectively. The residuals between the new reduced model and P2D model are much less than the original SP model errors. On the other hand, the reduction in computational burden of the rigourous model by using the proposed model is significant.

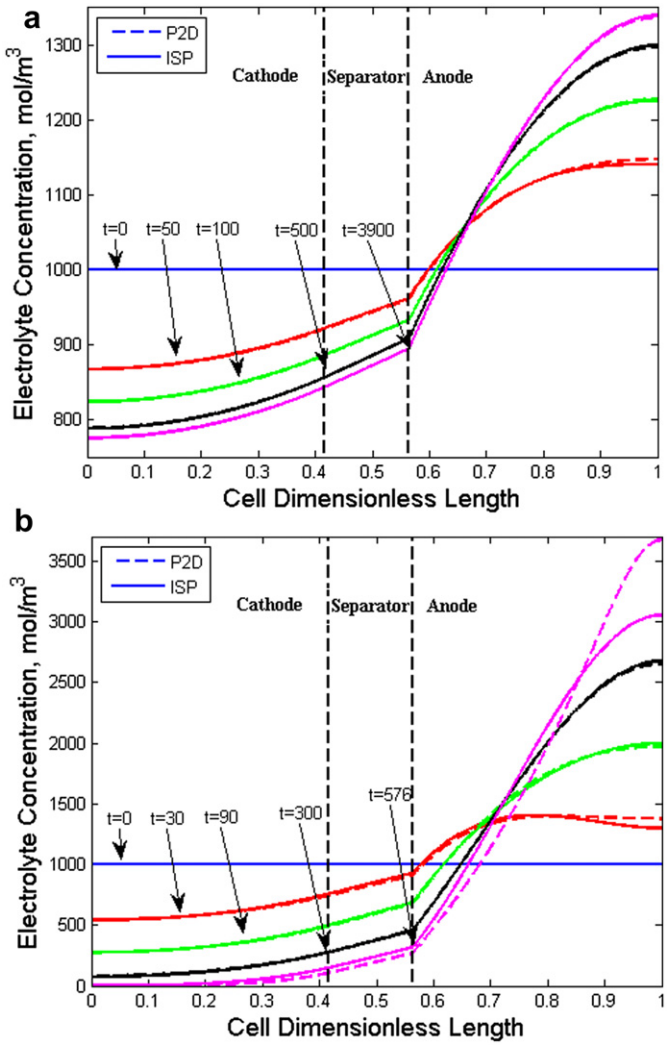

Fig. 10. Comparison electrolyte concentration obtained by ISP and P2D models during discharge (a) 1C (b) 5C.

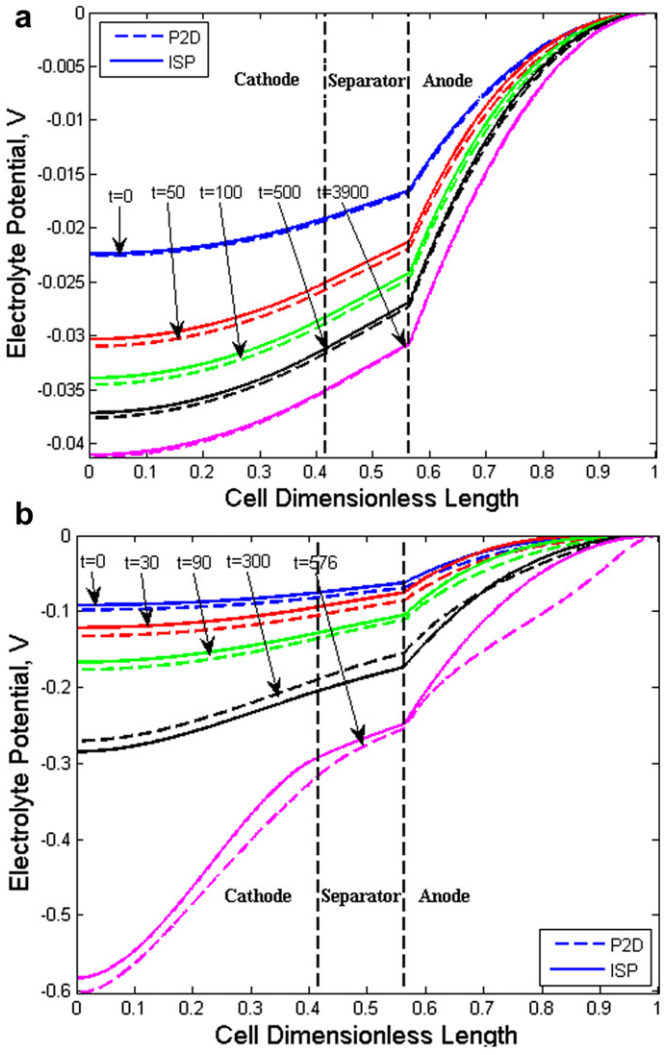

Fig. 11. Comparison electrolyte potential obtained by ISP and P2D models during discharge (a) 1C (b) 5C.

3.2. Electrolyte concentration

Li ion concentration in the solution phase inside the cell sandwich predicted by ISP model for 1C and 5C discharge rates is compared with electrolyte concentration obtained by P2D model in Fig. 10. Although, the new model prediction of the electrolyte concentration at 1C agrees well with the rigorous model, the prediction of ISP model at 5 C differs from the P2D model result. However, the errors in the solution phase concentration of the reduced model do not affect the cell voltage significantly as shown in Fig. 9. In order to improve the accuracy of ISP model electrolyte concentration, higher order polynomials can be applied.

3.3. Electrolyte potential

The comparison of solution phase potential inside the cell obtained by ISP and P2D models at 1C and 5C discharge rates is depicted in Fig. 11. At 1C, ISP model prediction agrees well with P2D model results (<0.001 V). However, the difference between the two models' potentials rises at 5C (~0.05 V) as shown in Fig. 11b. In spite of ISP model electrolyte potential deviation from the full order model, the cell voltage prediction of both model are in good agreement (<1%).

3.4. Solid concentration

Fig. 12 compares the P2D cell voltage at 5C charge–discharge rate with the reduced model where the volume average technique (dashed line) and the new approximation [18] (solid line) are used to predict the solid surface concentration. The improvement of the cell voltage prediction by applying the new approximation [18] instead of two term polynomial approximation is obvious especially at the beginning of charge (Fig. 12a) and the end of discharge (Fig. 12b).

3.5. Pore wall flux

The total flux of Li ions, J_i^T ($i = p,n$), does not change during constant current charge and discharge (e.g. for 1C, $\left|J_p^T\right| = \frac{I_{app}}{FS_p} = 1.5\times10^{-5}\ \frac{mol}{m^2 s}$, $\left|J_n^T\right| = \frac{I_{app}}{FS_n} = 2.3\times10^{-5}\frac{mol}{m^2 s}$). Nonetheless, the pore wall fluxes obtained by P2D and ISP models at interior points inside the electrodes (J_p^1, J_n^1) vary with time as presented in Figs. 13 and 14 for charge and discharge, respectively.

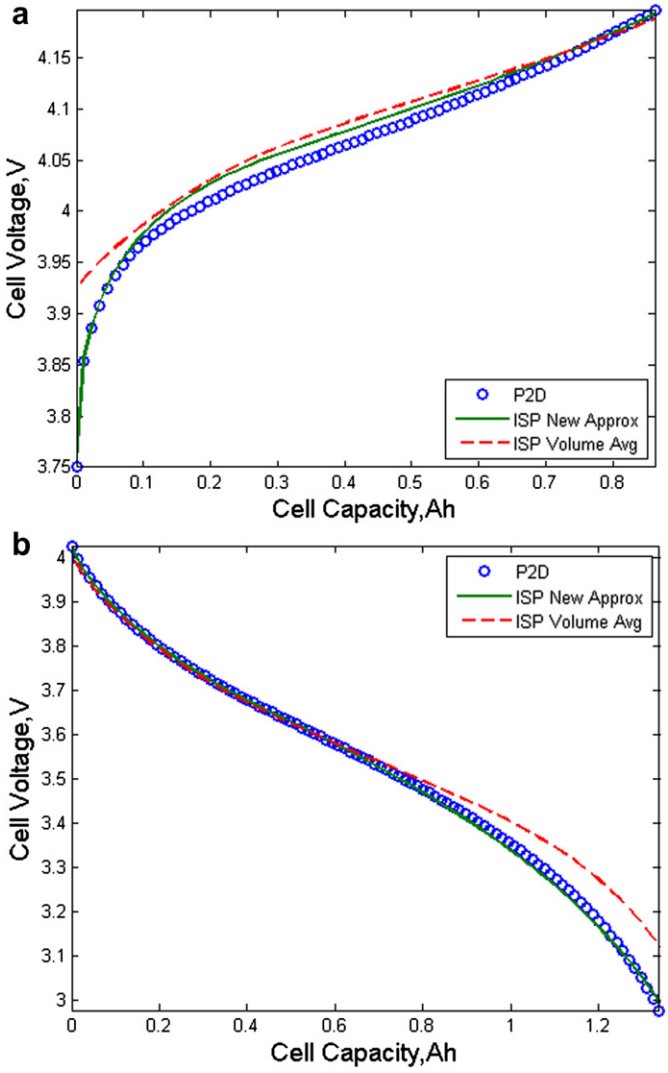

Fig. 12. Comparison of cell voltage at 5C obtained by P2D and ISP models where new approximation and volume average technique are used for solid concentration (a) charge (b) discharge.

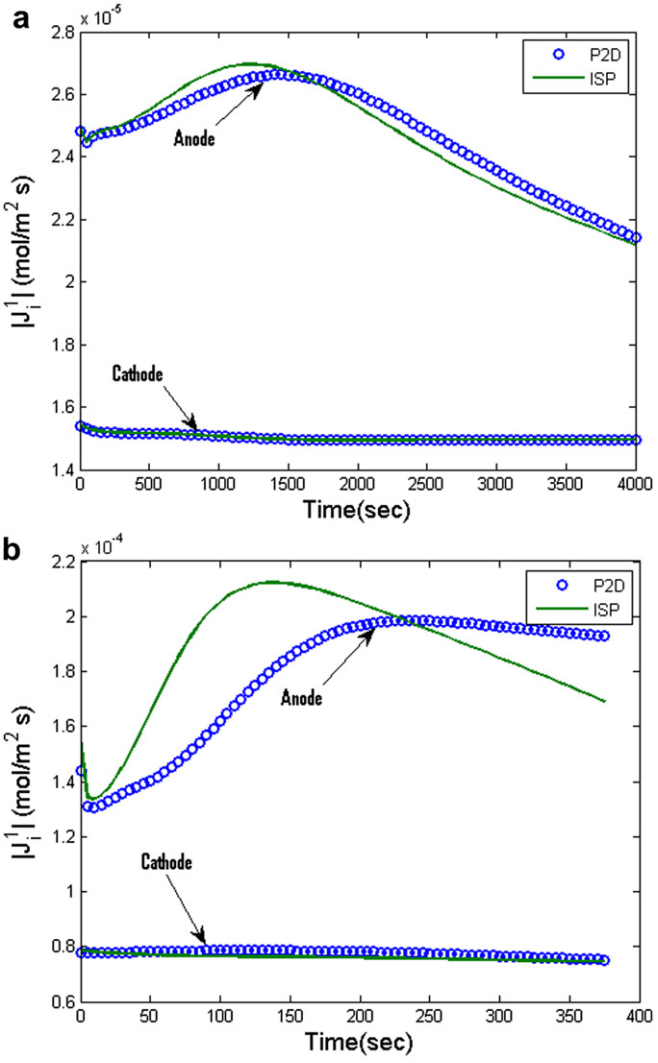

Fig. 13. Comparison of pore wall flux absolute values at interior points ($x_p^1 = 0.68$, $x_n^1 = 0.23$) obtained by ISP and P2D models during charge (a) 1C (b) 5C.

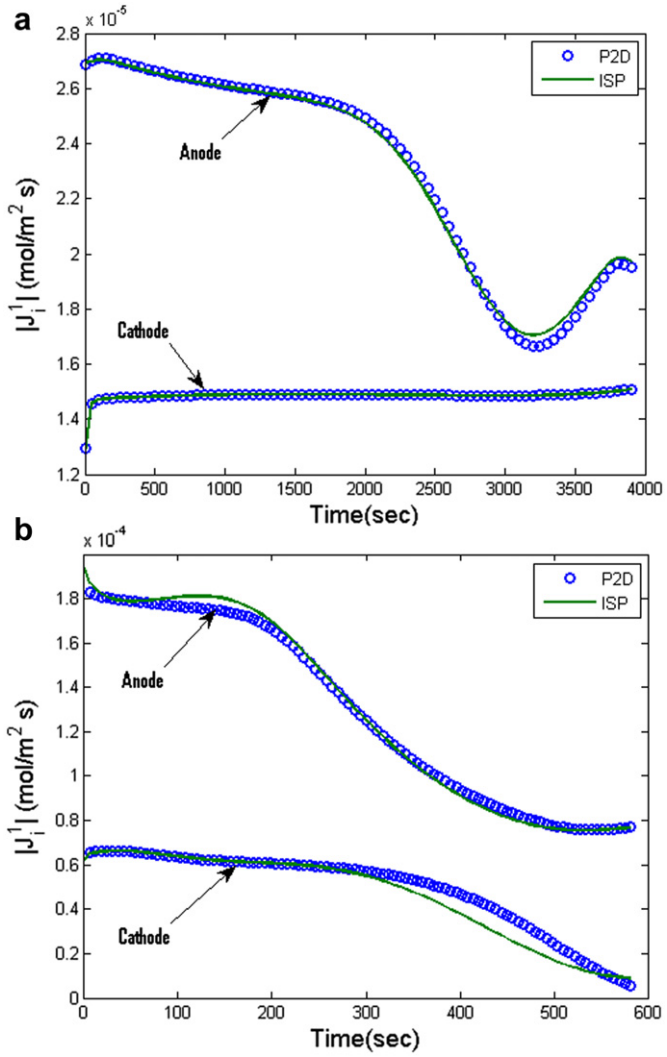

Fig. 14. Comparison of pore wall flux absolute values at interior points ($x_p^1 = 0.06$, $x_n^1 = 0.12$) obtained by ISP and P2D models during discharge (a) 1C (b) 5C.

The ISP model fluxes at 1C rate agrees well with the full order model fluxes as shown in Figs. 13a and 14a for charge and discharge, respectively. However, the difference between the fluxes of two models is considerable at 5C specifically for the negative electrode during charge (Fig. 13b). The pore wall flux error at the anode interior point can be described by Figs. 10b and 11b, where the ISP model electrolyte concentration and potential differs from the P2D model results. In order to improve the ISP model prediction of the interior pore wall flux inside the negative electrode higher order polynomial functions are required for the electrolyte concentration and potential (e.g. 4th order polynomial for $C_{e,n}$ and $\phi_{e,n}$). Note also that while the distribution of the electrolyte concentrations and potentials inside the cell can be provided by the ISP model, the pore wall flux can be obtained only at the interior points. Another point is that we also approximated the pore wall fluxes inside the electrodes by using polynomials profiles. Then, the solution phase potentials were obtained analytically by substituting the fluxes approximations in the electrolyte charge balances. However, the model results for electrolyte quantities deviated considerably with P2D model. Thus, polynomial approximation of the electrolyte potentials lead to more accurate reduced model rather than approximation of the pore wall fluxes.

4. Conclusion

An electrochemical based reduced order model has been proposed by improvement of the SP model. Neglecting solution phase electrochemical variations is the main error prone assumption of the SP model, resulting in significant error (>10%) in cell voltage prediction at higher rates (>1C). In the ISP model presented here, polynomial profiles are applied to approximate the Li ion concentrations and potential in the solution phase. The BV kinetic expression in the ISP model is both used in average form (like the original SP model) as well as at the optimal interior points for each electrode. The average concentrations and potentials are used in the former while the latter applies the concentrations and potentials at the interior points. Hence, pore wall fluxes inside the electrodes are no longer uniform in the new reduced ISP model. Using more accurate approximation for the solid phase diffusion rather than applying volume average technique, is another enhancement in ISP model. Comparison results shows that ISP model is able to predict the cell voltage less than 1% for different charge–discharge rates up to 5C, while the average computation cost is saved by a factor of 5.

References

[1] www.agmbatteries.com/documents/Lithium-ion_technology.pdf.
[2] D. Andrea, Battery Management Systems for Large Lithium-ion Battery Packs, Artech-House, MA, 2010.
[3] N.A. Chaturvedi, R. Klein, J. Christensen, J. Ahmed, A. Kojic, IEEE Control Systems Magazine (June 2010).
[4] M.W. Verbrugge, in: M. Schlesinger (Ed.), Modern Aspects of Electrochemistry, Modeling and Numerical Simulations I, vol. 43, Springer, New York, 2009.
[5] M. Doyle, T.F. Fuller, J. Newman, Journal of the Electrochemical Society 140 (1993) 1526–1533.
[6] T.F. Fuller, M. Doyle, J. Newman, Journal of the Electrochemical Society 141 (1994) 1–10.
[7] P. Ramadass, B. Haran, P.M. Gomadam, R.E. White, B.N. Popov, Journal of the Electrochemical Society 151 (2004) A196–A203.
[8] S. Atlung, K. West, T. Jacobsen, Journal of the Electrochemical Society 126 (1979) 1311–1321.
[9] B.S. Haran, B.N. Popov, R.E. White, Journal of Power Sources 75 (1998) 56–66.
[10] S. Khaleghi Rahimian, S. Rayman, R.E. White, Journal of Power Sources 196 (2011) 8450–8462.
[11] S. Santhanagopalan, Q. Guo, R.E. White, Journal of the Electrochemical Society 154 (2007) A198.
[12] V.R. Subramanian, V.D. Diwakar, D. Tapriyal, Journal of the Electrochemical Society 152 (2005) A2002–A2008.
[13] V.R. Subramanian, V. Boovaragavan, V.D. Diwakar, Electrochemical and Solid-State Letters 10 (2007) A255–A260.
[14] L. Cai, R.E. White, Journal of the Electrochemical Society 156 (2009) A154–A161.
[15] K.A. Smith, C.D. Rahn, C.Y. Wang, Energy Conversion and Management 48 (2007) 2565–2578.
[16] D.D. Domenico, A. Stefanopoulou, G. Fiengo, Journal of Dynamic Systems, Measurement, and Control 132 (2010) 061302.
[17] T.-S. Dao, C.P. Vyasarayani, J. McPhee, Journal of Power Sources 198 (2012) 329–337.
[18] M. Guo, R.E. White, Journal of Power Sources 198 (2012) 322–328.
[19] J. Newman, K.E. Thomas-Alyea, Electrochemical Systems, third ed., Wiley-Interscience, Hoboken, 2004.
[20] N. Lars Ole Valoen, Journal of the Electrochemical Society 152 (2005) A882–A891.
[21] C.Y. Wang, W.B. Gu, B.Y. Liaw, Journal of the Electrochemical Society 145 (1998) 3407.

List of symbols

a_i: specific interfacial area [1/m]
$brugg_i$: Bruggeman number
$C_{e,i}$: electrolyte concentration [mol m^{-3}]
$C_{s,i}$: solid phase concentration [mol m^{-3}]
$C_{s,max,i}$: maximum solid phase concentration [mol m^{-3}]
$D_{s,i}$: solid phase diffusion coefficient of Li^+ [m^2 s^{-1}]
$D_{e,i}$: electrolyte phase diffusion coefficient of Li^+ [m^2 s^{-1}]
F: Faraday's constant [C mol^{-1}]
I_{app}: applied current [C s^{-1}]
J_i: pore wall flux [mol m^{-2} s^{-1}]
$k_{e,i}$: electrolyte specific conductivity [S m^{-1}]
k_i: reaction rate constant [m$^{2.5}$ mol$^{-0.5}$ s^{-1}]
L: thickness of battery component [m]

m: polynomial order
Q_n: variable defined in Eq. (28b)
r: spatial coordinate
$\bar{r}$: dimensionless radius
R_g: gas constant [J mol^{-1}K^{-1}]
R_i: particle radius ($i = p, n$) [m]
S_i: electrode total active surface area [m^2]
t: time [s]
t_+^0: transference number of Li ions in electrolyte
T: temperature [K]
U_i: open circuit potential [V]
V_{cell}: cell voltage [V]
V_i: electrode volume [m^3]
x: spatial coordinate
$x_{s,avg,i}$: dimensionless solid average concentration
$x_{s,surf,i}$: dimensionless solid surface concentration
β: parameter defined in Eq. (6) ($\beta = 2R_gT(1-t_+^0)/F$)
$\sigma_{eff,i}$: effective solid conductivity [S m^{-1}]
η_i: electrode overpotential [V]
ϕ_i: electrode potential [V]
$\phi_{e,i}$: electrolyte potential [V]
ε_i: volume fraction of active material
$\varepsilon_{f,i}$: volume fraction of fillers
εL_{ps}: parameter defined in Eq. (20)
εL_{sn}: parameter defined in Eq. (20)
λ_n: eigenvalue
δ: dimensionless flux
τ: dimensionless time

Subscripts
0: initial condition
eff: efficient
max: maximum
n: negative electrode
p: positive electrode
s: separator

Superscripts
1: first interior point
T: total